Articles

The Oxotrifluoroxenon(VI) Cation: X-ray Crystal Structure of $XeOF_3^+SbF_6^-$ and a Solution ^{17}O and ^{129}Xe Nuclear Magnetic Resonance Study of the $^{17,18}O$-Enriched $XeOF_3^+$ Cation†

Hélène P. A. Mercier, Jeremy C. P. Sanders, Gary J. Schrobilgen,* and Scott S. Tsai

Department of Chemistry, McMaster University, Hamilton, Ontario L8S 4M1, Canada

Received June 2, 1992

The crystal structure of $XeOF_3^+SbF_6^-$ has been determined. The compound crystallized in the triclinic system with $a = 8.568$ (2) Å, $b = 9.760$ (2) Å, $c = 10.104$ (2) Å, $\alpha = 109.68$ (2)°, $\beta = 92.58$ (2)°, $\gamma = 104.27$ (2)°, $V = 763.4$ Å^3, and $D_{calc} = 3.829$ g cm^{-3} for $Z = 4$. The structure has been refined in the space group $P\bar{1}$ to a final conventional R factor of 0.045 for 1782 independent reflections with $I \geq 2.5\sigma(I)$. The structure consists of $XeOF_3^+SbF_6^-$ units with two close contacts between the Xe atom of the cation and F atoms of two SbF_6^- anions. The isolated $XeOF_3^+$ cation is shown to be consistent with the VSEPR rules and to possess an AX_4E arrangement of the four bond pair domains and the lone pair domain which give rise to a disphenoid-shaped cation having two longer axial Xe–F_{ax} bonds and an Xe–O bond which is coplanar with the shorter equatorial Xe–F_{eq} bond and xenon. Oxygen-17 and -18 enrichment of the $XeOF_3^+$ cation in HF and SbF_5 solvents has allowed the determination of the ^{17}O chemical shift and $^1J(^{129}Xe-^{17}O)$, as well as the $^{16,18}O$ induced secondary isotopic shift in the ^{129}Xe NMR spectrum for the first time.

Introduction

Xenon oxotetrafluoride was shown by Selig[1] to form the adduct $XeOF_4 \cdot 2SbF_5$, but its structure was not investigated at that time. The structural characterization of the adducts $XeOF_4 \cdot 2SbF_5$ and $XeOF_4 \cdot SbF_5$ was first reported from this laboratory,[2-4] and it was shown by ^{19}F NMR and Raman spectroscopy that the adducts were the salts $XeOF_3^+SbF_6^-$ and $XeOF_3^+Sb_2F_{11}^-$. The geometry of the $XeOF_3^+$ cation was in accord with the disphenoidal AX_4E geometry predicted by the VSEPR model. A synthetic and Raman spectroscopic study of $XeOF_3^+$ salts by Bartlett and coworkers[5] upheld these findings. Subsequently, the ^{129}Xe NMR spectrum of $XeOF_3^+$ was obtained in SbF_5 solvent using natural isotopic abundances.[6]

With the exception of XeF_3^+, XeF_5^+, and $F_5Xe\cdots F\cdots XeF_5^+$,[7] no X-ray crystal structures had been determined for the high-valent xenon cations and for the oxofluoro cations $XeOF_3^+$, XeO_2F^+,[2-4,8] and $FO_2Xe\cdots F\cdots XeO_2F^+$.[8] The present study reports the X-ray crystal structure of $XeOF_3^+SbF_6^-$. Although the ^{129}Xe and ^{19}F NMR spectra of the $XeOF_3^+$ cation have been obtained previously on natural abundance samples,[2,3,6] no ^{17}O NMR data had been reported; indeed the only oxo–xenon species for which ^{17}O NMR data had been reported were the neutral compounds $XeOF_4$ and XeO_2F_2.[9] Therefore, in beginning to build up a set of ^{17}O NMR data on oxo–xenon compounds for comparative and predictive purposes, it was of particular interest to obtain the ^{17}O NMR data for an oxo–xenon cation. To this end the preparation of $XeOF_3^+SbF_6^-$ enriched in ^{17}O and ^{18}O was undertaken in order to obtain the ^{17}O NMR spectrum and to observe the $^{16,18}O$ induced secondary isotope shift in the ^{129}Xe NMR spectrum.

Results and Discussion

X-ray Crystal Structure of $XeOF_3^+SbF_6^-$. Important bond lengths, angles and significant long contact distances for the $XeOF_3^+$ cations, together with bond lengths and angles for the SbF_6^- anions of the two molecules, which had to be defined in the $P\bar{1}$ space group, are listed in Table I. Details of the data collection parameters and other crystallographic information for $P\bar{1}$ space group are given in Table II. The final atomic coordinates and the equivalent isotropic thermal parameters are summarized in Table III. Figures 1 and 2 show the asymmetric unit of the crystal structure and the local environment around Xe(1), respectively.

The free $XeOF_3^+$ cation is predicted by the VSEPR model[13] to be a disphenoid with the oxygen atom, a fluorine atom, and the nonbonding electron pair in the equatorial plane and may be classed as an AX_4E arrangement of bond pairs (X) and a lone pair (E). The crystal structure shows essentially the geometry corresponding to this arrangement when the cation is considered in isolation from the anion. The location of the lone pair in the (Xe,O,F_{eq}) plane of the free cation may be inferred from the F_{ax}–Xe–F_{ax} bond angles F(5)–Xe(1)–F(1) and F(11)–Xe(2)–F(12) of 161.4 (5)° and 163.9 (5)°, respectively, and the F_{eq}–Xe–O bond angles O(1)–Xe(1)–F(2) and O(2)–Xe(2)–F(13) of 99.9 (6) and 100.9 (6)°, respectively. Both angle types are significantly less than the ideal angles (180 and 120°) expected in a trigonal bipyramid owing to axial fluorine–lone pair, and oxygen and equatorial fluorine bond pair–lone pair repulsions.

The structure of the $XeOF_3^+$ cation is similar to that of the isovalent $ClOF_3$ molecule.[14] As in $XeOF_3^+$, the equatorial F and

† Dedicated to Professor Neil Bartlett on the occasion of his 60th birthday.

(1) Selig, H. *Inorg. Chem.* **1966**, *5*, 183.
(2) Gillespie, R. J.; Landa, B.; Schrobilgen, G. J. *J. Chem. Soc., Chem. Commun.* **1972**, 607.
(3) Gillespie, R. J.; Schrobilgen, G. J. *Inorg. Chem.* **1974**, *13*, 2370.
(4) Gillespie, R. J.; Landa, B.; Schrobilgen, G. J. *Inorg. Chem.* **1976**, *15*, 1256.
(5) McKee, D. E.; Adams, C. J.; Bartlett, N. *Inorg. Chem.* **1973**, *12*, 1722.
(6) Schrobilgen, G. J.; Holloway, J. H.; Granger, P.; Brevard, C. *Inorg. Chem.* **1978**, *17*, 980.
(7) Selig, H.; Holloway, J. H. *Top. Curr. Chem.* **1984**, *124*, 33.
(8) Christe, K. O.; Wilson, W. W. *Inorg. Chem.* **1988**, *27*, 2714.
(9) Schumacher, G. A.; Schrobilgen, G. J. *Inorg. Chem.* **1984**, *23*, 2923.
(10) Brown, I. D. *J. Solid State Chem.* **1974**, *11*, 214.
(11) Brown, I. D. In *Structure and Bonding in Crystals*; O'Keefe, M., Navrotsky, A., Eds.; Academic Press: London, 1981; Vol. 2, p 1.
(12) Brown, I. D.; Altermatt, D. *Acta Crystallogr.* **1985**, *B41*, 244.
(13) Gillespie, R. J.; Hargittai, I. *The VSEPR Model of Molecular Geometry*; Allyn and Bacon: Boston, 1991.
(14) Oberhammer, H.; Christe, K. O. *Inorg. Chem.* **1982**, *21*, 273.

0020-1669/93/1332-0386$04.00/0

Table I. Bond Distances (Å), Bond Angles (deg) and Bond Valences in $XeOF_3^+SbF_6^-$

Bond Lengths (Å) and Corresponding Bond Valences (vu)[a]

	Xe(1)–F(1)	Xe(1)–F(2)	Xe(1)–F(5)	Xe(1)–F(3)[b]	Xe(1)–F(4)[b]	Xe(1)–O(1)
bond valence	0.98	1.22	1.07	0.18	0.22	2.18
bond length	1.896 (11)	1.818 (11)	1.864 (12)	2.535 (13)	2.449 (10)	1.682 (15)
tot. bond valence: 5.85						
	Xe(2)–F(12)	Xe(2)–F(13)	Xe(2)–F(11)	Xe(2)–F(9)[b]	Xe(2)–F(14)[b]	Xe(2)–O(2)
bond valence	1.02	1.20	1.05	0.15	0.17	2.07
bond length	1.885 (12)	1.824 (12)	1.871 (12)	2.589 (10)	2.541 (14)	1.701 (12)
tot. bond valence: 5.66						
	Sb(1)–F(4)	Sb(1)–F(6)	Sb(1)–F(7)	Sb(1)–F(8)	Sb(1)–F(9)	Sb(1)–F(10)
bond valence	0.68	0.84	0.81	0.87	0.80	0.89
bond length	1.940 (9)	1.863 (14)	1.877 (14)	1.847 (15)	1.881 (11)	1.839 (11)
tot. bond valence: 4.89						
	Sb(2)–F(14)	Sb(2)–F(16)	Sb(2)–F(18)	Sb(2)–F(15)	Sb(2)–F(17)	Sb(2)–F(3)
bond valence	0.76	0.87	0.92	0.89	0.84	0.73
bond length	1.899 (12)	1.850 (11)	1.827 (12)	1.842 (13)	1.863 (12)	1.912 (12)
tot. bond valence: 5.01						

	F(3)–Xe(1)	F(3)–Sb(2)		F(14)–Xe(2)	F(14)–Sb(2)
bond valence	0.18	0.73	bond valence	0.17	0.76
bond length	2.535 (13)	1.912 (12)	bond length	2.541 (14)	1.899 (12)
tot. bond valence: 0.91			tot. bond valence: 0.93		
	F(4)–Xe(1)	F(4)–Sb(1)		F(9)–Xe(2)	F(9)–Sb(1)
bond valence	0.22	0.68	bond valence	0.15	0.80
bond length	2.449 (10)	1.940 (9)	bond length	2.589 (10)	1.881 (10)
tot. bond valence: 0.90			tot. bond valence: 0.95		

Bond Angles (deg)

O(1)–Xe(1)–F(2)	99.9 (6)	O(1)–Xe(1)–F(1)	95.2 (6)	F(1)–Xe(1)–F(3)	88.4 (5)
F(3)–Xe(1)–F(4)	100.7 (4)	O(1)–Xe(1)–F(5)	92.5 (7)	F(3)–Xe(1)–F(5)	81.8 (5)
O(1)–Xe(1)–F(4)	84.2 (5)	F(1)–Xe(1)–F(2)	81.0 (5)	F(1)–Xe(1)–F(4)	122.9 (4)
F(2)–Xe(1)–F(3)	72.7 (4)	F(2)–Xe(1)–F(5)	81.0 (5)	F(5)–Xe(1)–F(4)	74.7 (4)
F(5)–Xe(1)–F(1)	161.4 (5)				
O(2)–Xe(2)–F(13)	100.9 (6)	O(2)–Xe(2)–F(11)	92.0 (6)	F(9)–Xe(2)–F(11)	74.1 (4)
F(9)–Xe(2)–F(14)	91.6 (4)	O(2)–Xe(2)–F(12)	92.1 (6)	F(9)–Xe(2)–F(12)	100.5 (4)
O(2)–Xe(2)–F(14)	87.3 (6)	F(11)–Xe(2)–F(13)	82.3 (5)	F(11)–Xe(2)–F(14)	73.7 (5)
F(9)–Xe(2)–F(13)	74.6 (5)	F(12)–Xe(2)–F(13)	81.7 (5)	F(12)–Xe(2)–F(14)	122.0 (5)
F(11)–Xe(2)–F(12)	163.9 (5)				

[a] Bond valence units (vu) are defined in refs 10–12. [b] Anionic fluorine atom bridge to a cationic xenon atom, only Xe–F contacts up to 3.55 Å were included.

Table II. Summary of Crystal Data and Refinement Results for $XeOF_3^+SbF_6^-$

space group	$P\bar{1}$	molecules/unit cell	4
a (Å)	8.568 (2)	mol wt	440.03
b (Å)	9.760 (2)	calcd density (g cm^{-3})	3.829
c (Å)	10.104 (2)	T (°C)	−89
α (deg)	109.68 (3)	μ (mm−1)	8.098
β (deg)	92.58 (3)	wavelength (Å) used for data collcn	0.560 87
γ (deg)	104.27 (3)	final agreement factors	R = 0.0452
V (Å^3)	763.4 (4)		R_w = 0.0632

O ligands in $ClOF_3$ are bent toward each other with a F_{eq}–Cl–O bond angle of 108.9°, and the axial ligands are bent back due to bond pair–lone pair repulsions to give an F_{ax}–Cl–F_{ax} bond angle of 170 (5)°. The structure of the $XeOF_3^+$ cation is also related to that of the XeF_3^+ cation[15,16] and can be described by replacement of one of the equatorial lone pairs by the oxygen atom. The F_{ax}–Xe–F_{ax} angles of XeF_3^+ are 160.9 (5) (SbF_6^- salt)[15] and 161.9 (5)° ($Sb_2F_{11}^-$ salt)[16] and are very similar to those of $XeOF_3^+SbF_6^-$ (161.4 (5) and 163.9 (5)°). This is in accord with a commonly observed equivalence in repulsive effect of an oxygen ligand and a nonbonding valence electron pair and is also seen in $XeOF_4$, in which the repulsive effect of the apical oxygen ligand balances that of the nonbonding pair so that the four F ligands and the Xe atom are almost coplanar, as in XeF_4.

Table IV lists the Xe–F and Xe–O bond lengths of a number of xenon fluorides and oxofluorides to allow comparison with the bond lengths found for $XeOF_3^+$. The Xe–O bond lengths for all of the species listed are similar, ranging from 1.682 (15) to 1.77 (1) Å. The average Xe-F bond length in $XeOF_3^+$ is shorter (1.860 (12) Å) than that found in $XeOF_4$ (1.900 (5) Å).[18] This is consistent with the trend found for XeF_3^+ (1.883 (13) Å;[15] 1.87 (1) Å[16]) and XeF_4 (1.953 (2) Å[22]) and is attributed to the decreased bond polarity resulting from the increased effective electronegativity of xenon as a result of its formal positive charge.[15] The Xe–F_{ax} bond lengths are longer than the Xe–F_{eq} bond lengths.

(15) Boldrini, P.; Gillespie, R. J.; Ireland, P. R.; Schrobilgen, G. J. *Inorg. Chem.* **1974**, *13*, 1690.
(16) McKee, D. E.; Zalkin, A.; Bartlett, N. *Inorg. Chem.* **1973**, *12*, 1713.
(17) Gavin, R. M., Jr.; Bartell, L. S. *J. Chem. Phys.* **1968**, *48*, 2460; *J. Chem. Phys.* **1968**, *48*, 2466.
(18) Martins, J.; Wilson, E. B., Jr. *J. Mol. Spectrosc.* **1968**, *26*, 410.
(19) Holloway, J. H.; Kaučič, V.; Martin-Rovet, D.; Russel, D. R.; Schrobilgen, G. J.; Selig, H. *Inorg. Chem.* **1985**, *24*, 678.
(20) Peterson, S. W.; Willet, R. D.; Huston, J. L. *J. Chem. Phys.* **1973**, *59*, 453.
(21) Templeton, D. H.; Zalkin, A.; Forrester, J. D.; Williamson, S. M. In *Noble Gas Compounds*; Hyman, H. H., Ed.; University of Chicago Press: Chicago, IL, 1963; p 203.
(22) Burns, J. H.; Agron, P. A.; Levy, H. A. In *Noble Gas Compounds*; Hyman, H. H., Ed.; University of Chicago Press: Chicago, IL, 1963; p 211.
(23) Levy, H. A.; Agron, P. A. In *Noble Gas Compounds*; Hyman, H. H., Ed.; University of Chicago Press: Chicago, IL, 1963; p 221.

Table III. Atomic Coordinates ($\times 10^4$) and Equivalent Isotropic Displacement Coefficients ($Å^2 \times 10^3$) for $XeOF_3^+SbF_6^-$

	x	y	z	U(eq)[a]
Xe(1)	4470 (1)	-2246 (1)	1293 (1)	19 (1)
O(1)	2941 (15)	-2029 (16)	350 (13)	33 (6)
F(1)	3286 (13)	-4141 (11)	1341 (12)	30 (4)
F(2)	5251 (13)	-3484 (12)	-138 (10)	30 (4)
F(3)	6997 (13)	-2603 (15)	2378 (12)	37 (5)
F(5)	6018 (14)	-778 (13)	894 (12)	36 (5)
Sb(1)	5589 (1)	2265 (1)	4114 (1)	19 (1)
F(4)	4387 (13)	179 (11)	3038 (12)	33 (4)
F(6)	5282 (14)	1917 (15)	5800 (12)	38 (5)
F(7)	7479 (14)	1610 (14)	4007 (12)	37 (5)
F(8)	5719 (14)	2533 (16)	2394 (13)	42 (6)
F(9)	3557 (12)	2679 (12)	4129 (11)	29 (4)
F(10)	6672 (16)	4264 (14)	5111 (15)	52 (6)
Xe(2)	710 (1)	2118 (1)	2754 (1)	21 (1)
O(2)	-962 (15)	1497 (16)	1511 (13)	29 (5)
F(11)	1714 (14)	758 (13)	1581 (12)	38 (5)
F(12)	121 (15)	3878 (12)	3781 (12)	37 (5)
F(13)	2074 (13)	3450 (13)	2129 (11)	34 (5)
Sb(2)	-738 (1)	-2488 (1)	2533 (1)	21 (1)
F(14)	-293 (15)	-346 (13)	3194 (12)	38 (5)
F(15)	-779 (15)	-2474 (15)	714 (12)	43 (5)
F(16)	1483 (13)	-2226 (15)	2759 (12)	40 (5)
F(17)	-820 (13)	-2359 (14)	4409 (11)	34 (5)
F(18)	-1231 (16)	-4554 (14)	1866 (14)	47 (5)

[a] Equivalent isotropic U defined as one-third of the trace of the orthogonalized U_{ij} tensor.

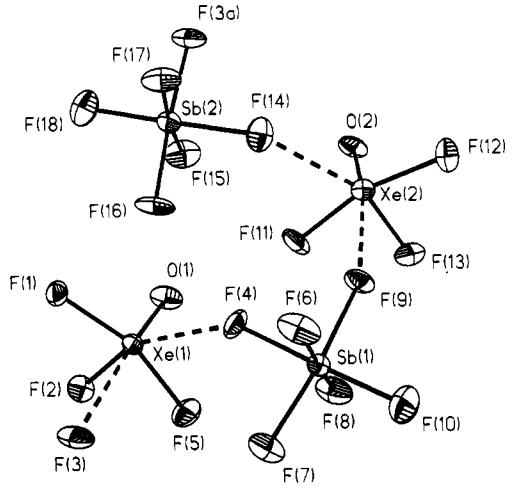

Figure 1. Asymmetric unit of the crystal structure of $XeOF_3^+SbF_6^-$; the long fluorine–bridge contacts are represented by dotted lines; thermal ellipsoids are shown at the 50% probability level.

This relates well with the data observed from the NMR study described below and can be explained in terms of bond order arguments. The bonding in the F_{ax}–Xe–F_{ax} unit can be regarded as a three-center–four-electron system with each Xe–F_{ax} bond having a bond order of $^1/_2$, whereas the Xe-F_{eq} bond is a two-center–two-electron bond with a bond order of 1. Thus the Xe–F_{eq} bond is stronger and shorter. The VSEPR model, which also predicts the Xe–F_{ax} bonds to be longer than the Xe–F_{eq} bond, does so without making any assumptions regarding the molecular orbitals used in bonding. Taking into account that the angle between the Xe,O,F_{eq} plane and the Xe–F_{ax} bond is less than the ideal angle of 90° and that the angle between the electron lone pair and the oxygen and fluorine equatorial ligands is considerably less than 120°, it is inferred that these distortions arise from lone pair–bond pair repulsions which are minimized by elongation of the Xe–F_{ax} bonds.

The crystal structure of $XeOF_3^+SbF_6^-$ also shows two nonequivalent long fluorine–bridge contacts from two different SbF_6^- anions to each $XeOF_3^+$ cation (Figures 1 and 2), giving distorted octahedral coordination around the xenon atom as in monomeric

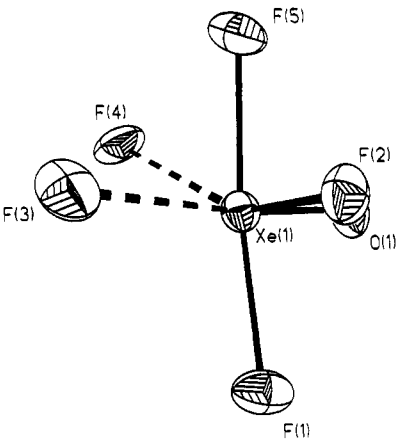

Figure 2. Local environment around xenon in $XeOF_3^+SbF_6^-$; only the Xe(1) environment is depicted.

Table IV. Xe–F and Xe–O Bond Lengths of Some Xenon Fluorides and Oxofluorides

	Xe–F (Å)	Xe–O (Å)	ref
XeF_6	1.890 (5)		16
$XeOF_4$	1.900 (5)	1.703 (2)	17
$XeOF_3^+SbF_6^-$	1.879 (12) (ax)	1.692 (13)	*a*
	eq 1.821 (12) (eq)		
$Cs^+(XeOF_4)_3F^-$	1.90 (3)[b]	1.70 (5)	18
XeO_2F_2	1.899 (3)	1.714 (4)	19
$K^+XeO_3F^-$	2.42 (1)[c]	1.77 (1)[d]	20
XeF_4	1.953 (2)		21, 22
$XeF_3^+SbF_6^-$	1.906 (14)[b] (ax)		14
	1.835 (10) (eq)		
$XeF_3^+SbF_6^-$	1.89 (1) (ax)		15
	1.83 (1) (eq)		
XeF_2	2.00 (1)		23

[a] This work. [b] Average value for the Xe–F bonds. [c] Average value for a Xe–F bond in which the F acts as a bridge between two xenon atoms. [d] Average value for the Xe–O bonds.

XeF_6.[17,24-26] A direct consequence of the two fluorine bridge interactions is a two-dimensional layer structure in which there are no close contacts between parallel layers (Figure 3). The long contact distances are 2.535 (13) Å for Xe(1)–F(3), 2.449 (10) Å for Xe(1)–F(4), 2.589 (10) Å for Xe(2)–F(9), and 2.541 (14) Å for Xe(2)–F(14). These contact distances are significantly less than the sum of the Xe and F van der Waals radii (3.50 Å)[27] and indicate that there is substantial covalent character in these interactions. The bond valences for individual bonds as defined by Brown[10-12] are included in Table I. Taking into account the two fluorine bridge contacts, the total bond valences for the Xe(1) and Xe(2) atoms are 5.85 and 5.66, respectively, and for the Sb(1) and Sb(2) atoms they are 4.89 and 5.01, respectively. The oxygen atoms O(1) and O(2) have bond valences values of 2.18 and 2.07, respectively, and the terminal fluorines have values of 0.98, 1.02 (F_{ax} on Xe), 1.05–1.22 (F_{eq} on Xe), and 0.81–0.92 (Sb). The bridge fluorine values range from 0.15 to 0.22 for the Xe contacts and from 0.80 to 0.68 for the Sb contacts giving total bridge fluorine bond valences of 0.95–0.90. The total bond valences of xenon and the bond valences of the bridging fluorine confirm that only two significant long contacts between the cation and the anion need to be taken into account.

(24) Cutler, J. N.; Bancroft, G. M.; Bozek, J. D.; Tan, K. H.; Schrobilgen, G. J. *J. Am. Chem. Soc.* **1991**, *113*, 9125.
(25) Rothman, M. J.; Bartell, L. S.; Ewig, C. S.; van Wazer, J. R. *J. Chem. Phys.* **1980**, *73*, 375.
(26) Pitzer, K. S.; Bernstein, L. S. *J. Chem. Phys.* **1975**, *63*, 3849 and references therein.
(27) Bondi, A. *J. Phys. Chem.* **1964**, *68*, 441.
(28) The NRCVAX Crystal Structure System: Larson, A. C.; Lee, F. L.; LePage, Y.; Webster, M.; Charland, J. P.; Gabe, E. J. Chemistry Division, NRC, Ottawa Canada. PC version: White, P. S. Department of Chemistry, University of North Carolina, Chapel Hill, N.C.

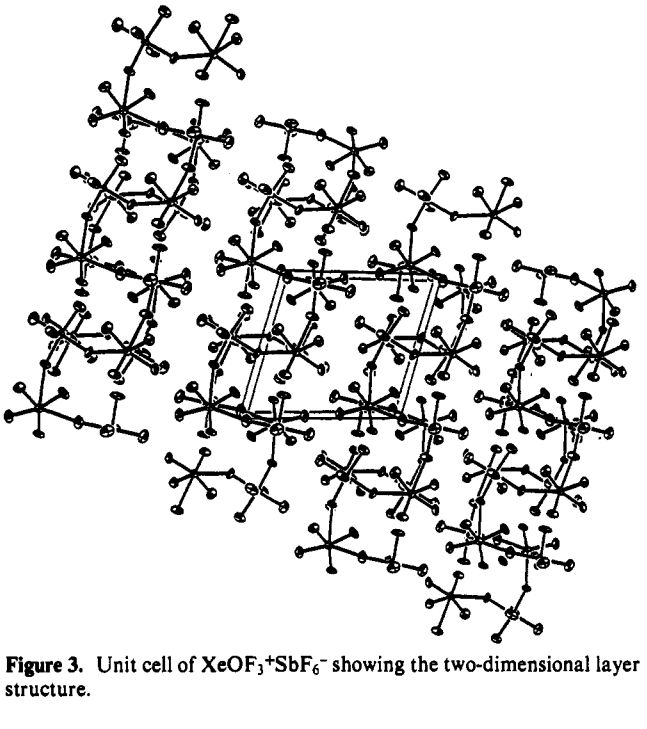

Figure 3. Unit cell of $XeOF_3^+SbF_6^-$ showing the two-dimensional layer structure.

Table V gives the equation for the least-squares planes containing the equatorial ligands O and F_{eq} and the Xe atom. The long fluorine bridge contacts with the SbF_6^- anion approach the Xe atoms from above the plane of the equatorial ligands. For both Xe(1) and Xe(2), it is evident that the shorter of the two long F- - -Xe contacts subtends the greater angle with the F_{eq}–Xe–O plane, i.e., F(4) (F(14)) subtends an angle of 24.13 (1)° (23.79 (1)°) to the F(2)–Xe(1)–O(1) (F(13)–Xe(2)–O(2)) plane while F(3) (F(9)) subtends an angle of 4.66 (1)° (13.36 (1)°) to the F(2)–Xe(1)–O(1) (F(13)–Xe(2)–O(2)) plane. The approaches of the bridging fluorines on the same side of the equatorial plane suggest that the nonbonding electron pair is displaced from the ideal equatorial (Xe,O,F_{eq}) plane of the AX_4E arrangement toward the least crowded triangular face (comprised of the two bridging fluorines and the equatorial fluorine in the AX_4E description of the isolated $XeOF_3^+$ cation). The lone pair avoids occupying a face-containing oxygen which would result in a more crowded environment for the lone electron pair domain. In fact, the triangular face containing the oxygen atom is compressed by the splaying open of the opposite face resulting from lone pair–bond pair repulsions in the pseudotrigonal face defined by the two long fluorine contacts and an axial fluorine (see Table I for relevant bond angles). Figure 4 shows a view down the axis passing through the triangular faces of the distorted octahedron, and is consistent with displacement of the long pair domain toward the triangular face directly below the xenon atom. Repulsion between the nonbonding electron pair and the bonding electron pairs causes the F(1)–F(3)–F(4) and F(9)–F(12)–F(14) triads to splay outwards. When the two long contacts are taken into account, the geometry resembles an AX_6E (distorted octahedral) arrangement akin to that of XeF_6 in the gas phase[24-26] except that the lone pair of $XeOF_3^+$ is not expected to be centered on the triangular face, but is expected to be displaced toward the lines of approach of the long Xe···F contacts.

One important difference between the structures of $XeOF_3^+SbF_6^-$ and $XeF_3^+SbF_6^-$ [15] is the direction of the secondary bonding interactions (fluorine bridges) between the cation and the anion. The directions of approach of these incoming electron pair(s) are dictated by their tendency to avoid the other electron pair(s) in the valence shell of xenon. Assuming that the arrangement of electron pairs around xenon in XeF_3^+ is a regular trigonal bipyramid, it was found that the directions of the secondary contacts in $XeF_3^+SbF_6^-$ were in agreement with the direction expected. They approach from above and below the equatorial lone pairs in the centers of the triangular faces defined by the axial fluorines and the lone pairs, passing through two triangular faces of the trigonal bipyramidal AX_3E_2 arrangement of the free cation to give an arrangement in which the Xe atom and five F atoms are coplanar.[15] Thus, the XeF_3^+ cation and its fluorine bridge contacts approximate an AX_5E_2 arrangement that is closely related to the regular pentagonal planar AX_5E_2 geometry of XeF_5^-.[29]

The SbF_6^- anions of $XeOF_3^+SbF_6^-$ have the usual octahedral geometry and expected Sb-F bond lengths ranging from 1.827 (12) to 1.940 (9) Å. The Sb–F bond length differences are attributed to fluorine bridge formation, so that the two unique pairs of fluorines involved in bridging (F(4), F(9); F(3), F(14) have slightly elongated Sb–F bonds (Table I) and the Sb–F bonds trans to the bridge bonds are slightly contracted; i.e., Sb(1)–F(10) = 1.839 (11), and Sb(1)–F(8) = 1.847 (15), Sb(2)–F(18) = 1.827 (12), and Sb(2)–F(15) = 1.842 (13) Å.

The vibrational spectrum of $XeOF_3^+SbF_6^-$ has been reported previously.[4] In view of the present crystal structure, a factor-group analysis of the vibrational modes of the $XeOF_3^+SbF_6^-$ unit cell was carried out by use of the correlation chart method.[30] The free cation symmetry (C_s) was correlated to the site symmetry of the cation (C_1), which, in turn, was correlated to the crystal symmetry (C_i). Assuming complete vibrational coupling occurs in the unit cell of $XeOF_3^+SbF_6^-$, 18 modes having A_g symmetry are predicted to be active in the Raman spectrum and 18 modes having A_u symmetry are predicted to be active in the infrared spectrum. Thus, each vibrational band of the free cation is predicted to be split in the Raman and infrared spectra. Such splittings have been noted in the previously published Raman spectra of $XeOF_3^+SbF_6^-$ [4,5] and can now be attributed to vibrational coupling within the unit cell. The totally symmetric Xe–F stretching modes all exhibited splitting. Although no splitting was resolved for the Xe–O stretching mode, reexamination of the Raman spectrum of $XeOF_3^+SbF_6^-$ under higher resolution conditions in the present study reveals a low-frequency shoulder at 2.8 cm^{-1} to low frequency of the main band.

Solution ^{129}Xe and ^{17}O NMR Study of the $XeOF_3^+$ Cation. The ^{17}O-enriched salt $XeOF_3^+SbF_6^-$ was prepared from ^{17}O-enriched $XeOF_4$ (oxygen composition: ^{16}O, 36.5%; ^{17}O, 26.5%; ^{18}O, 37.0%) according to eq 1. The $XeOF_3^+$ cation is expected

$$XeOF_4 + SbF_5 \xrightarrow{HF} XeOF_3^+SbF_6^- \qquad (1)$$

to act as a strong acceptor toward F^- donor solvents such as HF resulting in loss of the one-bond Xe–F couplings in the ^{129}Xe and ^{19}F NMR spectra due to rapid fluorine ligand exchange.[6] However, the Xe=O bond is not labile and HF is a good solvent in which to observe the ^{17}O NMR spectrum, because its low viscosity helps to minimize the quadrupolar relaxation of the ^{17}O nucleus.[31] In order to observe the Xe–F couplings in $XeOF_3^+$, it is necessary to dissolve $XeOF_3^+SbF_6^-$ in the very strong fluoroacid SbF_5. It has previously been demonstrated that the addition of XeF_2 to the SbF_5 not only enhances the solubility of $XeOF_3^+SbF_6^-$ in this medium due to the increased ionizing power of the solvent in the presence of XeF^+ and $Sb_nF_{5n+1}^-$ ions but also reduces its viscosity considerably, thereby allowing the observation of high-resolution spectra.[3]

The ^{129}Xe NMR spectrum at 30 °C of $XeOF_3^+SbF_6^-$ dissolved in HF and acidified with a 5-fold molar excess of AsF_5 (mole ratio of AsF_5:HF ≈ 1:20) is depicted in Figure 5a. The AsF_5 was

(29) Christe, K. O.; Curtis, E. C.; Dixon, D. A.; Mercier, H. P.; Sanders, J. C. P.; Schrobilgen, G. J. *J. Am. Chem. Soc.* **1991**, *113*, 3351.
(30) Carter, R. L. *J. Chem. Educ.* **1971**, *48*, 297 and references therein.
(31) Sanders, J. C. P.; Schrobilgen, G. J. In *Multinuclear Magnetic Resonance in Liquids and Solids – Chemical Applications*; Granger, P., Harris, R. K., Eds.; NATO ASI Series C, Kluwer Academic Publishers: Boston, MA, 1990; p 157.

Table V. Equations for the Equatorial Least-Squares Planes of $XeOF_3^+$ [a]

atoms in the plane	*A*	*B*	*C*	*D*	σ(*A*)		*d* (Å)[b]	angle ∥[c] (deg)	angle ⊥[d] (deg)
Xe(1),O(1),F(2)	3.741	7.407	−4.373	0.961	0.013	F(1)	−1.868		9.70
						F(5)	1.840		8.93
						F(3)	0.206	4.66	
						F(4)	1.001	24.13	
Xe(2),O(2),F(13)	−5.124	6.868	3.459	7.207	0.014	F(12)	1.865		8.31
						F(11)	−1.854		7.71
						F(9)	−0.598	13.36	
						F(14)	−1.025	23.79	

[a] Equations defined by $AX + BY + CZ = D$ in the direct crystal coordinate system; calculated by the program BESPLN from the NRCVAX package.[28] σ is the standard deviation. [b] Distances (Å) to the plane from the atoms out of the plane. [c] Angle (deg) with the plane. [d] Angle (deg) with the perpendicular to the plane.

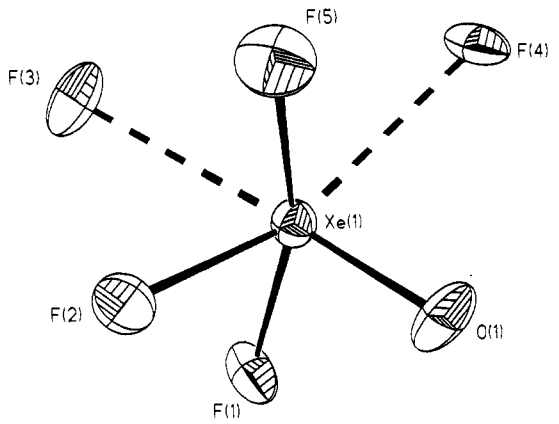

Figure 4. View down the axis passing through Xe(1) and the triangular faces F(2)–F(5)–O(1) and F(1)–F(3)–F(4) in the $XeOF_3^+$ cation; a very similar arrangement is observed for Xe(2).

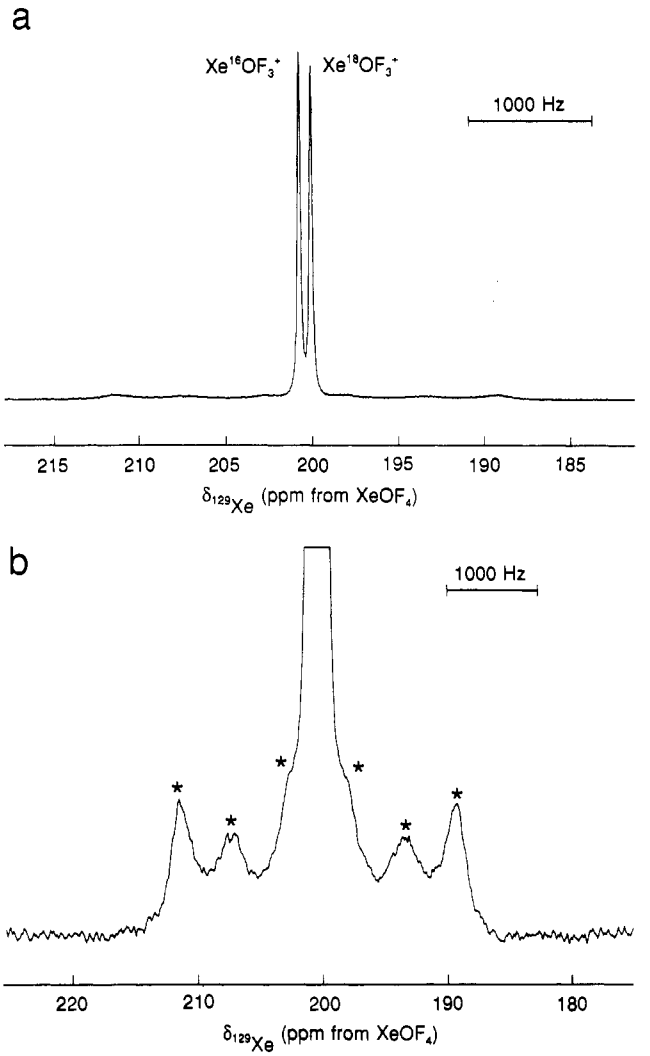

Figure 5. ^{129}Xe NMR spectrum (139.051 MHz) at 30 °C of the ^{17}O-(26.5%) and ^{18}O-enriched (37.0%) $XeOF_3^+$ cation: (a) $Xe^{16,17,18}OF_3^+SbF_6^-$ (ca. 0.5 M) in HF solvent acidified with AsF_5 (2.7 M); (b) vertical expansion (× 32) showing the coupling of ^{129}Xe to ^{17}O (denoted with asterisks) in the $Xe^{17}OF_3^+$ isotopomer.

added in an effort to slow the intermolecular fluoride exchange and allow the observation of the one-bond Xe–F couplings. This method has previously been used to slow the fluorine ligand exchange in the IF_6^+ and TeF_3^+ cations so that $^1J(^{19}F–^{127}I)$ and $^1J(^{19}F–^{125}Te)$ could be observed.[32,33] The ^{129}Xe spectrum displays two singlets of similar intensity at 200.8 and 200.1 ppm attributable to the $Xe^{16}OF_3^+$ and $Xe^{18}OF_3^+$ isotopomers, respectively. The difference in chemical shift between the two isotopomers [$^1\Delta^{129}Xe(^{18,16}O)$, −0.69 ppm] represents the first observation of a secondary isotope shift in a xenon oxofluoro cation. At high gain (Figure 5b) the broad equal-intensity sextet of the $Xe^{17}OF_3^+$ isotopomer can be seen. The multiplet arises from the coupling of ^{129}Xe to the ^{17}O ($I = {}^5/_2$) and shows the expected variation in component line widths for a quadrupolar nucleus undergoing modestly slow relaxation. The average $^{129}Xe–^{17}O$ coupling constant measured from this spectrum was 545 Hz; no coupling between Xe and the F ligands was observed, indicating that intermolecular fluorine exchange is still rapid even in the presence of an excess of the strong fluoro-acid AsF_5. The ^{17}O NMR spectrum of the same sample (Figure 6) shows a singlet ($\Delta\nu_{1/2}$, 132 Hz) at 333.7 ppm with flanking ^{129}Xe satellites [$^1J(^{17}O–^{129}Xe)$, 619 Hz] attributable to the $Xe^{17}OF_3^+$ cation. The smaller value of $^1J(^{17}O–^{129}Xe)$ measured in the ^{129}Xe NMR spectrum as compared with that measured in the ^{17}O NMR spectrum is attributable to the partial quadrupole collapse of the equal-intensity sextet in the ^{129}Xe spectrum, which results in a symmetrical variation in the spacings between the components of the sextet.[31] This means that an accurate value of the $^{129}Xe–^{17}O$ coupling cannot be measured from this spectrum without computer simulation.[31] However, the $^1J(^{17}O–^{129}Xe)$ value obtained from the ^{17}O NMR spectrum is reliable, since the separation between the ^{129}Xe satellites is independent of the different lifetimes of the ^{17}O spin states.[34] The ^{129}Xe NMR spectrum of a mixture of $XeOF_3^+SbF_6^-$ and XeF_2 (1:5.3 mole ratio) in neat SbF_5 is depicted in Figure 7a. The spectrum displays two broad partly overlapping doublets of triplets ascribed to the $Xe^{16}OF_3^+$ and $Xe^{18}OF_3^+$ isotopomers at 237.4 and 238.0 ppm, respectively. When the spectrum is resolution enhanced by Gaussian multiplication of the FID, the two multiplets corresponding to the two isotopomers are clearly distinguished (Figure 7b). The secondary isotope shift, $^1\Delta^{129}Xe(^{18,16}O)$, was measured as −0.59 ppm. The multiplet pattern arises from the coupling of the ^{129}Xe to the unique equatorial fluorine ligand [$^1J(^{129}Xe–^{19}F_{eq})$, 1012 Hz] and

(32) Brownstein, M.; Selig, H. *Inorg. Chem.* **1972**, *11*, 656.
(33) Collins, M. J.; Schrobilgen, G. J. *Inorg. Chem.* **1985**, *24*, 2608.
(34) Bacon, J.; Gillespie, R. J.; Hartman, J. S.; Rao, U. K. K. *Mol. Phys.* **1970**, *18*, 561.

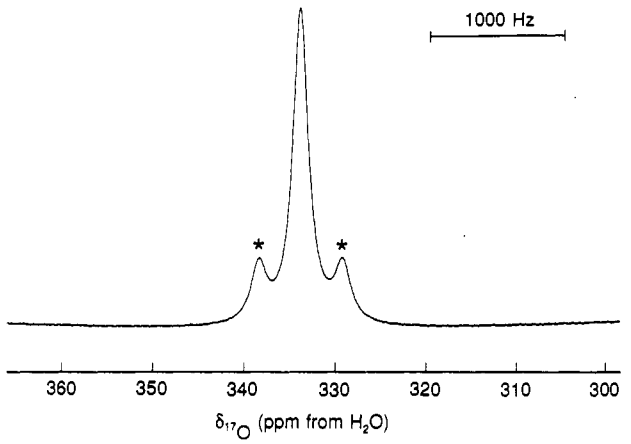

Figure 6. ^{17}O NMR spectrum (67.801 MHz) at 30 °C of ^{17}O- (26.5%) and ^{18}O-enriched (37.0%) $XeOF_3^+SbF_6^-$ (ca. 0.5 M) in HF solution acidified with AsF_5 (2.7 M). Asterisks denote ^{129}Xe satellites.

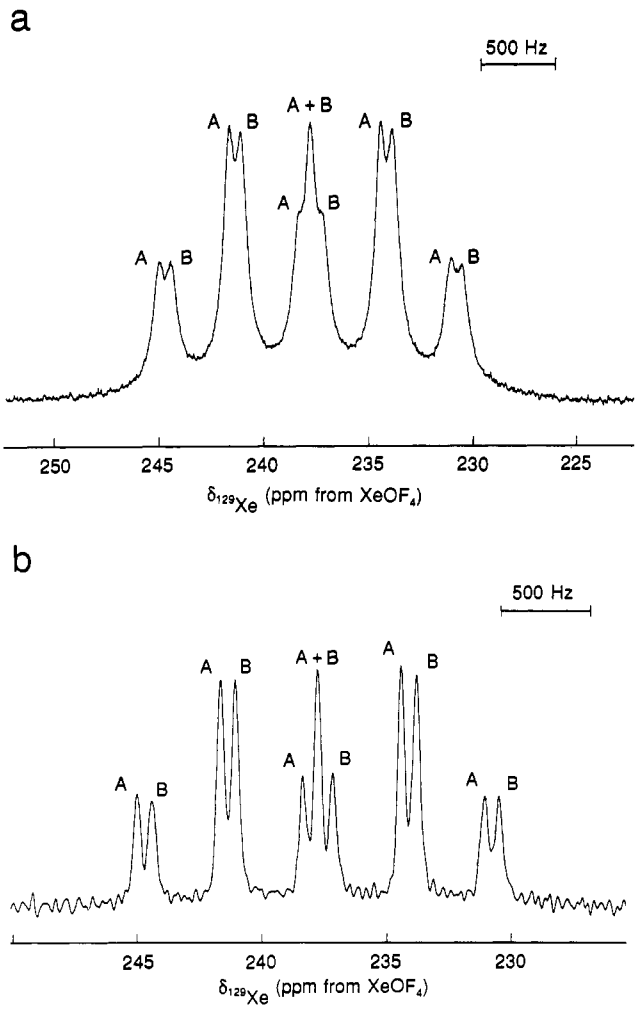

Figure 7. ^{129}Xe NMR spectrum (139.051 MHz) at 30 °C of ^{17}O- (26.5%) and ^{18}O-enriched (37.0%) $XeOF_3^+SbF_6^-$ (0.33 M) and XeF_2 (1.7 M) dissolved in SbF_5 solvent: (a) spectrum obtained by Fourier transformation of the free induction decay using a Lorentzian fit; (b) resolution enhanced spectrum obtained by Fourier transformation of the free induction decay using a Gaussian fit. A = $Xe^{16}OF_3^+$; B = $Xe^{18}OF_3^+$.

the two axial fluorine ligands [$^1J(^{129}Xe-^{19}F_{ax})$, 464 Hz]. These values are in reasonable agreement with those previously obtained on natural abundance samples of $XeOF_3^+SbF_6^-$.[3,6] The larger magnitude of $^1J(^{129}Xe-^{19}F_{eq})$ as compared with $^1J(^{129}Xe-^{19}F_{ax})$ is in good agreement with the prediction, based on simple MO ideas, that the Xe–F_{eq} bond will be stronger (bond order 1) than the Xe–F_{ax} bonds (bond order $^1/_2$) and fits in well with the shorter Xe–F_{eq} bond length obtained from the crystal structure determination (see earlier discussion). A resonance attributable to the $Xe^{17}OF_3^+$ isotopomer was not observed presumably owing to the much faster quadrupolar relaxation of the ^{17}O nucleus in the more viscous SbF_5 solution, which would result in the resonance being collapsed into the base line. Accordingly, the ^{17}O NMR spectrum of the sample shows a very broad ($\Delta\nu_{1/2}$, 5370 Hz) singlet at 342 ppm with no resolved ^{129}Xe satellites.

The new NMR data obtained for $XeOF_3^+$ can be compared with those previously obtained for $XeOF_4$ and XeO_2F_2,[9] although more data are required from other oxo–xenon species in order to draw firmer conclusions. The values of $^1\Delta^{129}Xe(^{18,16}O)$ obtained for the $XeOF_3^+$ cation are of the same magnitude as those measured for $XeOF_4$ [$^1\Delta^{129}Xe(^{18,16}O)$, –0.58 ppm][9] and XeO_2F_2 [$^1\Delta^{129}Xe(^{18,16}O)$, –0.52 ppm].[9] The ^{17}O chemical shift of the $XeOF_3^+$ in HF is deshielded relative to that of $XeOF_4$ [$\delta(^{17}O)$, 316.3 ppm], in accord with the increased positive charge on the cation.[35] Interestingly, the $^{129}Xe-^{17}O$ coupling in $XeOF_3^+$ is significantly smaller than the corresponding coupling in $XeOF_4$ [$^1J(^{129}Xe-^{17}O)$, 704 Hz][9] which, if it is assumed that the Fermi contact coupling mechanism provides the dominant contribution to the coupling constant, indicates a lower s-character in the Xe=O bond of the cation. However, this interpretation may not be justified in the light of recent experimental results, which suggest that the noncontact contributions to the coupling constant, namely, the spin–orbital and spin–dipolar terms, can provide an important contribution to coupling constants involving heavy nuclei.[36] This is especially likely to be the case where a multiple bond exists between the two coupled nuclei, such as in the Xe=O bond.[37,38] Unfortunately, there is insufficient data at present to allow unequivocal interpretation of the trends observed in the coupling constants of such systems. Further ^{17}O NMR studies on oxo–xenon compounds are currently in progress in this laboratory.

Conclusions

The X-ray crystal structure of $XeOF_3^+SbF_6^-$ demonstrates that the isolated $XeOF_3^+$ cation essentially adopts the disphenoidal geometry predicted by the VSEPR model for an AX_4E system with the oxygen atom, a fluorine atom, and the lone electron pair in the equatorial plane. The Raman spectroscopic data are in agreement with this finding. The fluorine bridge contacts between the cation and anion give rise to an AX_6E system that has the distorted monocapped octahedral geometry also predicted by the VSEPR model.

The ^{17}O NMR study on $XeOF_3^+SbF_6^-$ is only the third such study on an oxo–xenon compound and has yielded $\delta(^{17}O)$, $^1J(^{17}O-^{129}Xe)$ and $^1\Delta^{129}Xe(^{18,16}O)$ for the $XeOF_3^+$ cation for the first time. Interpretation of trends in these parameters will require the gathering of further ^{17}O data from other oxo–xenon species in order that useful comparisons might be made.

Experimental Section

Apparatus and Materials. All manipulations were performed under strictly anhydrous conditions in a nitrogen-filled drybox (Vacuum Atmospheres Model DLX) or on a vacuum line constructed from 316 stainless steel, nickel, Teflon, and FEP. Preparative work was carried out in $^1/_4$-in.-o.d. lengths of FEP tubing which were heat-sealed at one end and connected through 45° SAE flares to Kel-F valves.

Xenon oxotetrafluoride enriched in ^{17}O and ^{18}O was prepared as previously described[9] using enriched water (ORIS, Saclay, France) with the following oxygen composition: ^{16}O, 36.5%, ^{17}O, 26.5%, and ^{18}O, 37.0%.

(35) Jameson, C. J.; Mason, J. In *Multinuclear NMR*; Mason, J., Ed.; Plenum Press: New York, 1987; Chapter 3, p 66.
(36) Power, W. P.; Lumsden, M. D.; Wasylishen, R. E. *J. Am. Chem. Soc.* **1991**, *113*, 8257 and references therein.
(37) Jameson, C. J. In *Multinuclear NMR*; Mason, J., Ed.; Plenum Press: New York, 1987; Chapter 4, p 116.
(38) Cogne, A.; Grand, A.; Laugier, J.; Robert, J. B.; Wiesenfeld, L. *J. Am. Chem. Soc.* **1980**, *102*, 2238.

Arsenic pentafluoride was prepared by the fluorination of AsF_3[39] in a nickel can. The AsF_3 (35.61 g, 0.2699 mol) was distilled in vacuo into a 1-L nickel can equipped with a stainless steel Autoclave Engineers valve. Fluorine (0.4064 mol, 50% excess) was condensed into the can at −196 °C. The can was allowed to warm (*Caution! potentially hazardous reaction; safety shielding is advisable*) to room temperature and then heated to 163 °C overnight. The product was cooled to −196 °C and the excess fluorine pumped away through a soda lime trap. The AsF_5 was distilled into a nickel storage cylinder from which it was used without further purification.

The method used for the preparation of xenon difluoride was similar to that used by Malm and Chernick[40] for the preparation of XeF_4. In a typical preparation, xenon (0.236 mol) and fluorine (0.118 mol) were condensed into a nickel can (249 mL) at −196 °C. The can and contents were then allowed to warm to room temperature. At room temperature, the total pressure was estimated to be 34 atm. An electric furnace, preheated to 400 °C, was placed around the nickel can and maintained at this temperature for 7 h. The initial autogeneous pressure in the can at 400 °C was estimated to be 78 atm. After the specified time period, the furnace was removed and the nickel vessel and contents were rapidly quenched to room temperature in water. The can was cooled to −78 °C, and excess xenon was condensed into a storage cylinder at −196 °C. The XeF_2 was collected by pumping the contents of the nickel reaction vessel through a cold trap at −78 °C. The yield of XeF_2 was 19.86 g. (99.3%). The purity of the product was checked by recording the Raman spectrum in the range 450–600 cm^{-1}. Xenon difluoride has a strong line at 496 cm^{-1} whereas the most likely impurity, XeF_4, has two strong lines at 502 and 543 cm^{-1}. The amount of XeF_4 found in any of the preparations was generally estimated to be less than 0.5%.

Literature methods were used for the purification of HF (Harshaw Chemical Co.)[41] and SbF_5 (Ozark-Mahoning Co.).[42]

Synthesis of $Xe^{16,17,18}OF_3^+SbF_6^-$. Antimony pentafluoride (0.5162 g, 2.382 mmol) was syringed into a prefluorinated $^1/_4$-in.-o.d. FEP tube in a dry nitrogen-filled glovebag. The tube was fitted with a Kel-F valve and anhydrous HF (ca. 0.7 mL) distilled on to the SbF_5 at −196 °C. The HF and SbF_5 were mixed thoroughly at room temperature. The resulting solution was frozen to −196 °C and a slight excess of $Xe^{16,17,18}OF_4$ (0.55188 g, 2.4607 mmol) distilled into the tube. The sample was allowed to warm to room temperature to give a clear colorless solution. The volatile materials were pumped off at −40 °C. The product was pumped for several hours at 0 °C to yield $Xe^{16,17,18}OF_3^+SbF_6^-$ as a fine white, crystalline solid (1.0442 g, 99.4%).

NMR Sample of $Xe^{16,17,18}OF_3^+SbF_6^-$ in HF Acidified with AsF_5. A 9-mm o.d. FEP tube was loaded with $Xe^{16,17,18}OF_3^+SbF_6^-$ (0.3391 g, 0.7689 mmol) in the drybox. The tube was attached to the metal vacuum line and anhydrous HF (ca. 1.5 mL), followed by AsF_5 (4 mmol), distilled in at −196 °C. The tube was heat-sealed at −196 °C and stored in liquid nitrogen until the NMR spectra could be run.

NMR Sample of $Xe^{16,17,18}OF_3^+SbF_6^-/XeF_2$ in Neat SbF_5. Antimony pentafluoride (ca. 2 mL) was syringed into a 9-mm FEP tube in a dry nitrogen-filled glovebag. The tube was taken into the dry box and cooled to −196 °C in order to freeze the SbF_5. The $Xe^{16,17,18}OF_3^+SbF_6^-$ (0.2889 g, 0.6551 mmol) was added on top of the solid SbF_5. The sample was allowed to warm to room temperature to give a viscous suspension. Xenon difluoride (0.5937 g, 3.507 mmol) was added to the mixture and slowly dissolved with agitation over a period of 2 h. A clear yellow, mobile solution resulted. The tube was heat-sealed at −196 °C and stored in liquid nitrogen until the NMR spectra could be run.

Crystal Structure Determination of $XeOF_3^+SbF_6^-$. Crystal Growing. Approximately 100 mg of $XeOF_3^+SbF_6^-$ was transferred to a vacuum-dried 8-mm glass tube equipped with a brass bellows valve, the tube evacuated, and the bottom of the tube immersed in 40 °C water inside a glass dewar. The compound sublimed over a period of several hours, resulting in deposits of crystalline material on the tube walls above the water level. The tube was then transferred to a drybox equipped with a microscope and the crystals were removed by cutting open the glass tube and prying them off the walls with an iridium stylus. The crystals were colorless thick plates and were sealed in 0.1, 0.2, and 0.3-mm Lindemann glass capillaries and stored at −10 °C prior to mounting on the diffractometer. A preliminary observation of the sealed crystals under a polarized microscope revealed that some of them were twined. The crystal used in this study was a plate with dimensions 0.2 × 0.3 × 0.05 mm.

Collection and Reduction of X-ray Data. The crystal was centered on a Syntex $P2_1$ diffractometer. Accurate cell dimensions were determined at $T = -89$ °C from a least-squares refinement of the setting angles (χ, ϕ, and 2θ) obtained from 21 accurately centered reflections (with $16.82° \leq 2\theta \leq 29.21°$) chosen from a variety of points in reciprocal space. The examination of the peak profiles revealed single but slightly broadened peaks. Integrated diffraction intensities were collected using a θ–2θ scan technique with scan rates varying from 1.5 to 14.65°/min (in 2θ) so that the weaker reflections were examined most slowly to minimize counting errors. The data were collected with $0 \leq h \leq 11$, $-12 \leq k \leq +12$ and $-13 \leq l \leq +13$ and with $5 \leq 2\theta \leq 40°$, using silver radiation monochromatized with a graphite crystal ($\lambda = 0.560\ 87$ Å). During data collection the intensities of three standard reflections were monitored every 97 reflections to check for crystal stability and alignment. A total of 3219 reflections were collected out of which 102 were standard reflections. A total of 2911 unique reflections remained after averaging of equivalent reflections. A total of 1782 reflections, satisfying the condition $I \geq 2.5\sigma(I)$, were used for structure solution. The intensities of the standards dropped regularly to about 90% of their original values during the course of the data collection; this decomposition was later corrected by scaling the data linearly between each set of standards. Corrections were made for Lorentz and polarization effects. Absorption corrections were applied by using the program DIFABS[43] which also corrected for the crystal decay.

Crystal Data. The compound, F_9OSbXe (fw = 440.03 g mol^{-1}), crystallizes in the triclinic system, space group $P\bar{1}$, with the following crystal data at $T = -89$ °C: $a = 8.569$ (2) Å, $b = 9.760$ (2) Å, $c = 10.104$ (3) Å, $\alpha = 109.68$ (2)°, $\beta = 92.58$ (2)°, $\gamma = 104.27$ (2)°, $V = 770$ Å^3, and $D_{calc} = 3.83$ g cm^{-3} for $Z = 4$. Ag(Kα) radiation ($\lambda = 0.560\ 87$ Å, μ(Ag Kα) = 42.8 cm^{-1}) was used.

Solution and Refinement of the Structure. The XPREP program[44] was used for determining the correct cell and space group. It first confirmed the original cell and that the lattice was triclinic primitive. The structure was shown to be centrosymmetric by an examination of the *E*-statistics (calculated, 0.969; theoretical, 0.968), and consequently the structure was solved in the space group $P\bar{1}$. The choice of the space group $P\bar{1}$ was confirmed later on by using the program MISSYM,[44] which did not find any other symmetry.

A first solution was obtained without absorption corrections, and it was achieved by conventional heavy-atom Patterson methods, which located the positions of the heavy atoms. The four atoms were assigned antimony scattering factors. The full-matrix least-squares refinement of the antimony atom positions and isotropic thermal parameters gave a conventional agreement index $R\ (=\sum\|F_o\| - |F_c\|/\sum|F_o|)$ of 0.20. Resulting differences in the stereochemistry about the four heavy atoms clearly indicated the nature of each atom. A difference Fourier synthesis revealed the remaining fluorine and oxygen atoms and confirmed the choice of the antimony and xenon atoms. Refinement of positional and isotropic temperature parameters for all atoms (the oxygen atom being assigned a fluorine scattering factor) converged at $R = 0.13$.

At this stage, it was possible to distinguish, in each xenon environment, one bond length which was significantly shorter than the other ones, indicating the existence of a Xe–O bond. A significant improvement of the structure was achieved by introducing anisotropic thermal parameters for the four heavy atoms (Xe and Sb) and isotropic thermal parameters for the O and F atoms; the *R* factor dropped to $R = 0.084$. At that point, the examination of the F_o and F_c values revealed that, in general, the F_o values were smaller than the F_c values, indicating that isotropic corrections for secondary extinction needed to be included in the refinement. The introduction of a weighting factor ($w = 1/\sigma^2(F) + 0.006617F^2$) gave a final solution with $R = 0.053$ ($R_w = 0.055$).

The structure was solved a second time using data that had been corrected for absorption. The initial model used the atomic coordinates and isotropic thermal parameters defined previously for the Xe, Sb, F, and O atoms. The solution obtained ($R = 0.053$) indicated a significant improvement over that obtained without absorption corrections ($R = 0.082$). The structure was slightly improved by introducing anisotropic thermal parameters for the Xe and Sb atoms ($R = 0.048$). The F and O atoms could also be refined with anisotropic thermal parameters (*R*

(39) Hoffman, C. J. *Inorg. Synth.* **1953**, *4*, 150.
(40) Malm, J. G.; Chernick, C. L. *Inorg. Synth.* **1966**, *8*, 254.
(41) Emara, A. A. A.; Schrobilgen, G. J. *Inorg. Chem.* **1992**, *31*, 1323.
(42) Gillespie, R. J.; Netzer, A.; Schrobilgen, G. J. *Inorg. Chem.* **1974**, *13*, 1455.
(43) Walker, N.; Stuart, D. *Acta Crystallogr.* **1983**, *A39*, 158.
(44) Sheldrick, G. M. SHELXTL PLUS Release 4.21/V. Siemens Analytical X-Ray Instruments, Inc., Madison, WI, 1990.

= 0.045). The final refinement was obtained by introducing a weight factor ($w = 1/\sigma^2(F) + 0.004295F^2$) and an isotropic correction for secondary extinction, and gave rise to a residual, R, of 0.045 (R_w = 0.049). In the final difference Fourier map, the maximum and the minimum electron densities were +1.8 and −1.3 eÅ^3.

All calculations were performed on a 486 personal computer using the SHELXTL PLUS[43] determination package for structure solution and refinement as well as structure determination molecular graphics.

Nuclear Magnetic Resonance Spectroscopy. All spectra were recorded unlocked (field drift < 0.1 Hz h^{-1}) on a Bruker AM-500 spectrometer equipped with an 11.744-T cryomagnet and an Aspect 3000 computer. The spectra were obtained using a 10-mm broad-band VSP probe (tunable over the range 23–202 MHz) which was tuned to 67.801 and 139.051 MHz to observe ^{17}O and ^{129}Xe, respectively. Free induction decays for ^{17}O were accumulated in an 8K memory with a spectral width setting of 15 kHz, yielding an acquisition time of 0.270 s and a data point resolution of 3.70 Hz/data point. Free induction decays for ^{129}Xe were accumulated in 8K and 16K memories with spectral width settings of 15 and 30 kHz, respectively. These yielded acquisition times of 0.270 and 0.278 s and data point resolutions of 3.70 and 3.59 Hz/data point, respectively. No relaxation delays were applied. Typically, 9000–15000 transients were accumulated. The pulse widths corresponding to a bulk magnetization tip angle, θ, of approximately 90° were 6.4 μs (^{17}O) and 18 μs (^{129}Xe). Line broadening parameters used in the exponential multiplication of the free induction decays were set equal to the data point resolution of the spectrum.

The ^{17}O and ^{129}Xe NMR spectra were referenced to neat external samples of H_2O and $XeOF_4$, respectively, at ambient temperature (30 °C). The chemical shift convention used is that a positive (negative) sign indicates a chemical shift to high (low) frequency of the reference compound.

The NMR samples were prepared in 25-cm lengths of 9-mm-o.d. FEP plastic tubing as described previously[29] and stored at −196 °C until the spectra could be run.

Acknowledgment. We thank the U.S. Air Force Phillips Laboratory, Edwards Air Force Base, CA, for support of this work under Contract F04611-91-K-0004 and the Natural Sciences and Engineering Research Council of Canada for support in the form of an operating grant.

Supplementary Material Available: A structure determination summary (Table 6), anisotropic thermal parameters (Table 7), and stereoview ORTEP of the packing in the unit cell (Figure 8) (5 pages). Ordering information is given on any current masthead page. A tabulation of the observed and calculated structure factors (Table 8) (7 pages) is available upon request from G.J.S. up to 1 year from the date of publication.